*Central European Journal of Energetic Materials*, **2009**, *6*(1), 67-102.
ISSN 1733-7178

# Recent Trends in Research on Energetic Materials at Cambridge

William G. PROUD, Stephen M. WALLEY*,
David M. WILLIAMSON, Adam L. COLLINS
and John W. ADDISS

*SMF Fracture and Shock Physics Group, Cavendish Laboratory, J.J. Thomson Avenue, Cambridge CB3 0HE, United Kingdom*
**E-mail: smw14@cam.ac.uk*

**Abstract:** Recent work in our laboratory has established a time-temperature superposition law for a PBX. This was achieved by performing uniaxial compression testing over a wide range of strain rates and temperatures along with Differential Thermal Mechanical Analysis (DMTA). The classic WLF (Williams, Landel, Ferry) transform was found not to fit the shift factor needed to align the data whereas a simple log-linear fit did. The thermal properties (diffusivity, conductivity, heat capacity) of a PBX have been measured three different ways and found to agree (within experimental error) with the classic equation relating these three parameters. This gives us confidence that, for example, hot-spot ignition mechanisms of this class of energetic materials can be accurately modelled using their measured thermal properties. A modular instrumented testing facility has been designed and built to simulate and control the conditions experienced by novel heavy-metal-free (green) primers contained within ammunition. Physical data obtained from the facility, when compared with data from live fire tests, will give a greater understanding of which characteristics are important to functionality. As explosives are granular materials, the techniques developed for studying such materials are being applied to determine the effect of particle size distribution and shape on sensitivity.

**Keywords**: Differential Mechanical Thermal Analysis, DMTA, polymer bonded explosive, PBX, thermal properties, thermal diffusivity, thermal conductivity, green primers, green explosives, time-temperature equivalence, strain rate, EDC37, RDX, gap test, drop-weight, particle size distribution

# Introduction

The literature on mechanical energy release mechanisms of energetic materials is vast, amounting to many tens of thousands of papers and reports. By comparison, only a few hundred papers have been published on the shock or high strain rate properties of solid or powdered energetic materials considered simply as materials.

However, it is increasingly desired to model the impact response of structures (e.g. artillery shells, rockets) containing energetic materials using numerical methods [1, 2]. If meaningful numerical results are going to be obtained, it is important that constitutive relations are constructed which describe the mechanical response of unreacted energetic materials over the temperature and strain rate ranges of interest. With increasing concern about safe-handling, performance during use, changes in properties during storage, and transport of reactive materials, this area is presently amongst the most important in energetic materials research.

Also of importance to numerical modelling are the thermal properties of this class of materials as this governs hot spot development and hence the buildup to deflagration and/or detonation.

**Time-temperature superposition**

Recently much progress has been made in establishing the nature of the relationship between the temperature and the frequency/strain rate response of both energetic materials and their inert simulants [3, 4]. It has been shown in these studies that the character of the mechanical response of polymer-bonded explosives (PBXs), for example, is governed by the polymer binder (Figure 1). One of the most important parameters is the adhesion between the energetic crystals and the binder. Above the binder's glass transition, cracks usually go around the crystals ([5]; see also Figure 2*a*) whereas below the glass transition, the stiffness of the binder becomes comparable to that of the explosive so that cracks also propagate through the crystals (see Figure 2*b*). This may have important consequences for sensitivity if the deformation is such that the crystal fracture surfaces rub against one another.

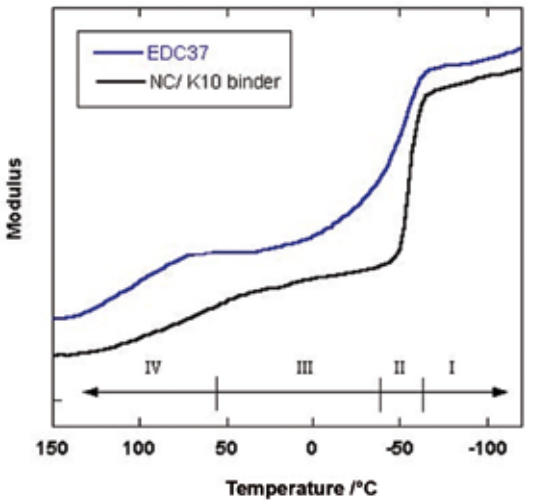


**Figure 1.** Storage modulus traces of binder and EDC37 powder samples obtained using Differential Mechanical Thermal Analysis (DMTA). Region I is the glassy state, region II is the glass transition region, region III is the rubbery plateau and region IV is viscous flow [3].

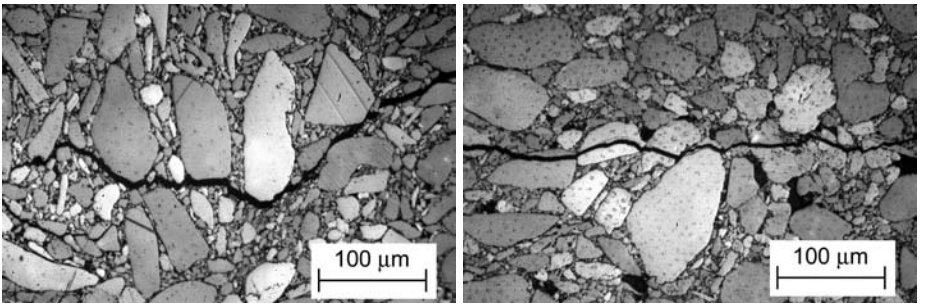


(*a*) (*b*)

**Figure 2.** (*a*) Micrograph of a mode I crack propagating through an energetic material where the temperature is above the glass transition of the binder. (*b*) Micrograph of a mode I crack propagating through an energetic material where the temperature is below the glass transition of the binder [5].

Figure 3 presents stress-strain curves for a particular PBX (EDC 37) obtained over 8 decades in strain rate. The data was obtained using six different machines in three different laboratories. It can be clearly seen that the strain rate has a strong effect on the yield and flow stresses, but no effect (within experimental

error) on the failure strain. These curves are all very interesting, but what is the mechanism that governs this behaviour? This became clearer when the failure stress was plotted as a function of strain rate (Figure 4) and compared with a plot of the failure stress obtained at one (low) strain rate over a range of temperatures (Figure 5). As before the failure strain did not vary systematically with temperature (Figure 6). As explained later, this last observation is important for understanding what is going on.

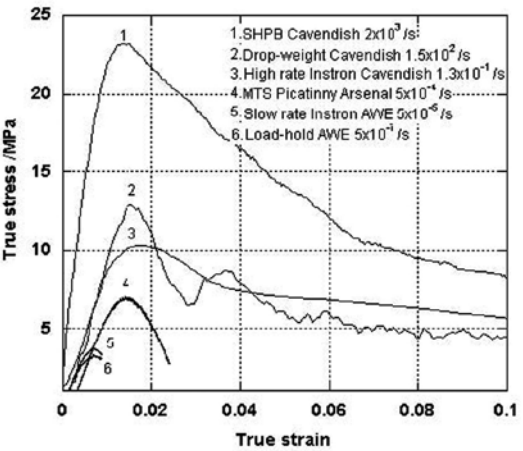


**Figure 3.** Typical results from the isothermal experimental techniques performed at 293K (from Ref. [3]).

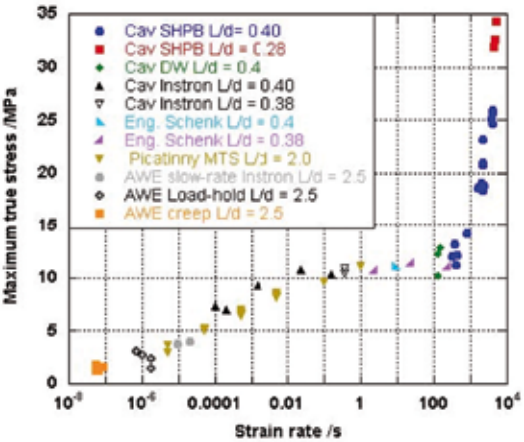


**Figure 4.** EDC37 failure stress as a function of strain rate tested at 293K (from Ref. [3]).

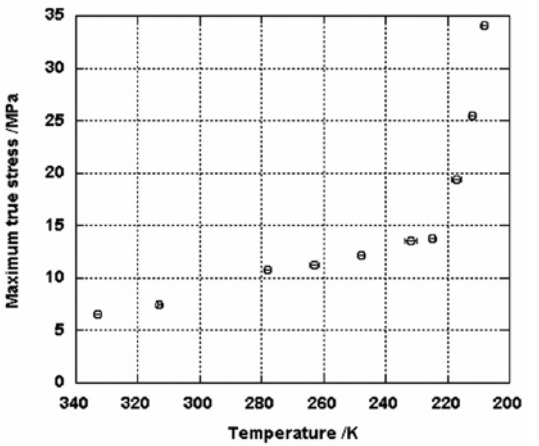


**Figure 5.** Fixed $10^{-3}$ $s^{-1}$ data: failure stress as a function of temperature (from Ref. [3]).

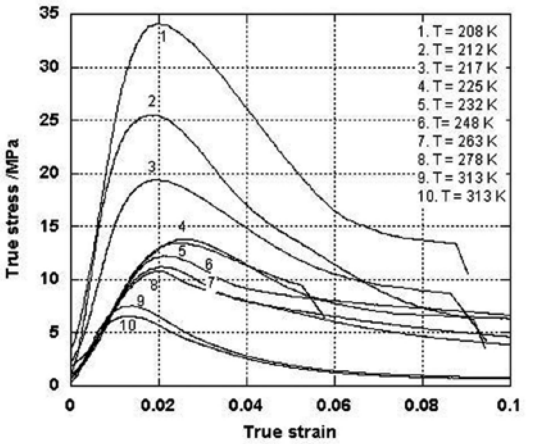


**Figure 6.** Typical results from the experiments performed at a strain rate of $10^{-3}$ $s^{-1}$ (from Ref. [3]).

The similarity in shape suggests some sort of time-temperature superposition, made familiar to us through the classic paper on polymers by Williams, Landel & Ferry [6], usually referred to as the WLF theory. Can this be quantified? Figure 7 is a plot of the data from Figure 5 superimposed on the data as that presented in Figure 4. It can be seen that a measure of the strain rate shift factor needed is $\Delta \log_{10}(\dot{\varepsilon})$. This shift factor was measured for a number of different temperatures (one example is shown in Figure 7) and plotted in Figure 8. The WLF theory

can be seen not to fit the data whereas a simple linear fit does. The equation describing this linear fit is:

$$\frac{\Delta \log_{10}(\dot{\varepsilon})}{\Delta T} = const. \tag{1}$$

The data yielded a time/temperature sensitivity of -13.1 ±0.3 K per decade of strain rate. This allows the data obtained by changing the temperature at a constant strain rate to be mapped onto the data obtained by changing the strain rate at a constant temperature (see Figure 9).

What is the reason time-temperature equivalence works for these materials? As commented on before, it can be seen in Figures 3 and 6 that the failure strain (stress peak) is almost insensitive to both temperature and strain rate. Thus to a first approximation the failure stress is proportional to the storage modulus, which can be measured using techniques such as DMTA. This explains the similarity between the schematic DMTA traces shown in Figure 1 and the real data shown in Figure 4.

If this is so, why is it still necessary to perform relatively expensive tests over a range of strain rates? Why not just do DMTA over a range of temperatures and use the rate/temperature equivalency to determine the mechanical properties, perhaps just doing a few (cheap) experiments at low rates to calibrate the stresses? The main reasons are the following: (i) different relaxation peaks may have different temperature sensitivities, and (ii) changing the temperature produces internal stresses in a specimen of energetic material due to the difference in thermal expansion coefficients of the binder and explosive crystals. These internal stresses can damage the material, changing its mechanical response. Temperature also changes the overall density of the material, which has been shown to affect the strength [7].

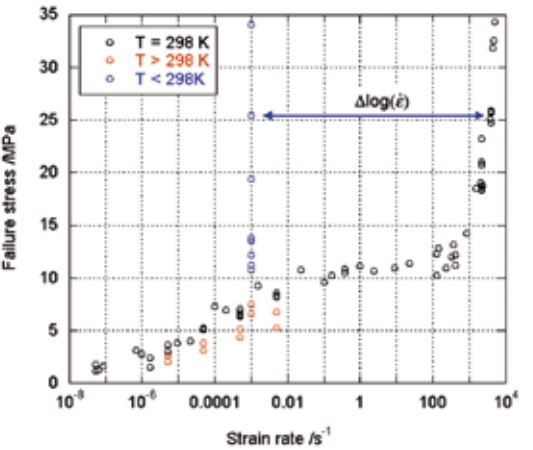


**Figure 7.** Graphical determination of $\Delta\log_{10}(\dot{\varepsilon})$.

It should be noted that the tensile fractures shown in Figure 2 were obtained by the indirect tensile (or Brazilian) method in which a disc of material is compressed across its diameter. Using optical techniques developed in our laboratory [8-10] and a numerical algorithm developed initially by Sjödahl & Benckert [11] a surface strain-field map can be determined (Figure 10*a*). This can be compared with the theoretical strain field (Figure 10*b*) calculated using the relations derived by Awaji & Sato [12]. The technique was developed originally for concrete by some Brazilian researchers [13] (hence the name) and is widely used to measure the tensile strength of materials such as concrete where it is difficult to make a conventional tensile specimen or (in the case of PBXs) where a dangerous amount of material would be needed to make such a specimen, let alone machine it.

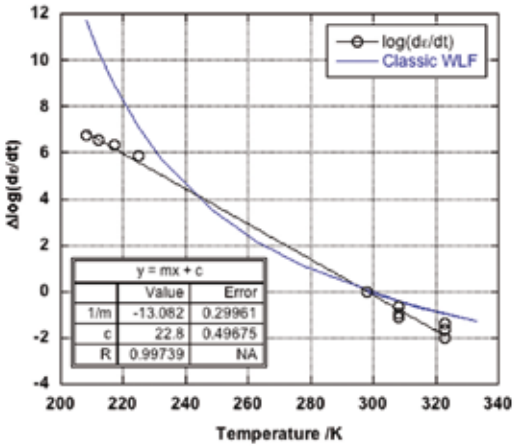


**Figure 8.** Strain rate shift factor, referenced to the glass transition temperature Tg as a function of applied temperature (from Ref. [3]).

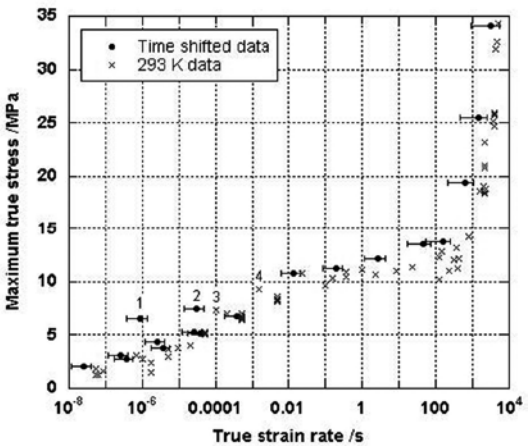


**Figure 9.** Application of time-temperature superposition principle using a linear transformation of -13.1 Kelvin per decade of strain rate. Data points 1 to 4 are of lower aspect ratio than the surrounding data in this region (from Ref. [3]).

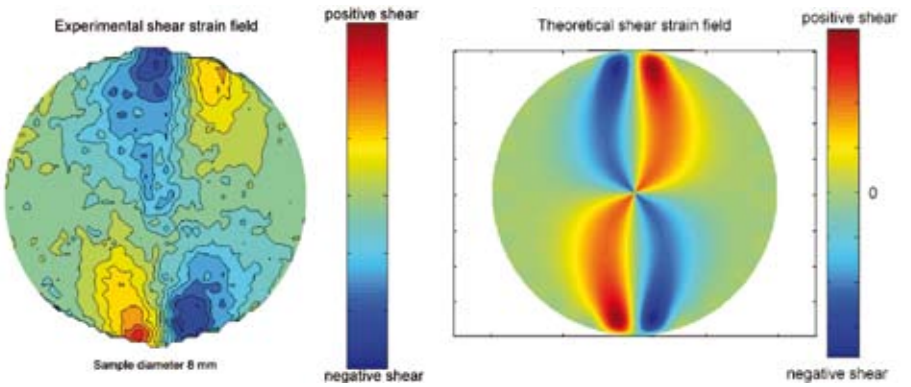


(*a*) (*b*)

**Figure 10.** Comparison of experiment (*a*) with theory (*b*) for the shear produced by diametral compression of a PBX disc.

**Thermal properties**

The thermal properties of an energetic material are required for the development and validation of thermal models related to the formation and growth of hot spots that eventually lead to deflagration and/or detonation [14]. Again the UK PBX EDC37 was studied. The aim was to independently determine the thermal conductivity $\kappa$, the thermal diffusivity $D$, and the heat capacity $C_p$ [15]. These parameters are related by the standard equation give in Ref. [16]:

$$D = \frac{\kappa}{\rho C_p} \tag{2}$$

where $\rho$ is the density. Hence a comparison between the measured value and that calculated from the other two gives an indication of the reliability of the data.

Thermal conductivity measurements were performed using Lees disc method [17] and described in many standard textbooks on experimental physics. In our version, this involves sandwiching a thin sample of EDC37 (25x25x3 mm) between two copper discs resting on a heating block that is set up to supply power at a constant rate. The temperature gradient is measured when the apparatus reaches thermal equilibrium. This allows the thermal conductivity to be calculated using the following equation due to Price & Jarrett [18]:

$$\kappa = \frac{ed}{A_S(T_B - T_A)}\{a_A T_A\} \tag{3}$$

where $T_A$ & $T_B$ are the temperatures of the copper plates above and below the specimen, $a_A$ is the exposed area of the copper plates, $A_S$ is the area of the specimen normal to the heat flow, $d$ is the sample thickness, and $e$ is the coefficient of convective heat transfer. A check on the accuracy of the method was performed using a variety of materials that have been well characterized in the literature. The data obtained is presented in Figure 11.

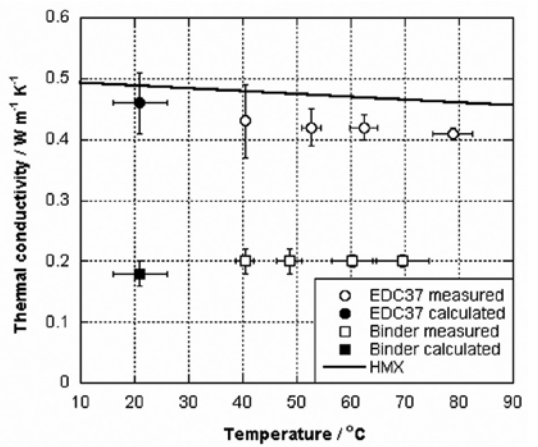


**Figure 11.** Thermal conductivity results. HMX data taken from Ref. [14].

Thermal diffusivity was investigated using a modification of Ångström's method [19-21] where a periodic heat cycle (period 240 s in our experiments) was applied using a Peltier cell to one face of a rectangular block of EDC37 (dimensions 12.7x12.7x127 mm). The progress of the thermal excursions above and below room temperature was monitored using a thermal imaging system (FLIR model SC3000). Examples of false colour images obtained using this system are presented in Figure 12. The system was checked using thermocouples. Figure 13 presents quantitative data obtained using the thermal imaging system. The two profiles were taken at two different and known distances from the Peltier junction: those shown in red were closer, those shown in blue were further away. The phase and amplitude at the two positions contain all the information needed to calculate $D$ using the following equation:

$$D = Lv / 2\ln \delta \tag{4}$$

where $v$ is the velocity with which the temperature wave travels, $L$ is the distance between two measurement points, and $\delta$ is the ratio of the temperature amplitude

at these two points [22]. A series of measurements were made over a range of temperatures and these are presented in Figure 14.

The heat capacity was measured using the standard technique of Differential Scanning Calorimetry (DSC). The data obtained using this technique is presented in Figure 15.

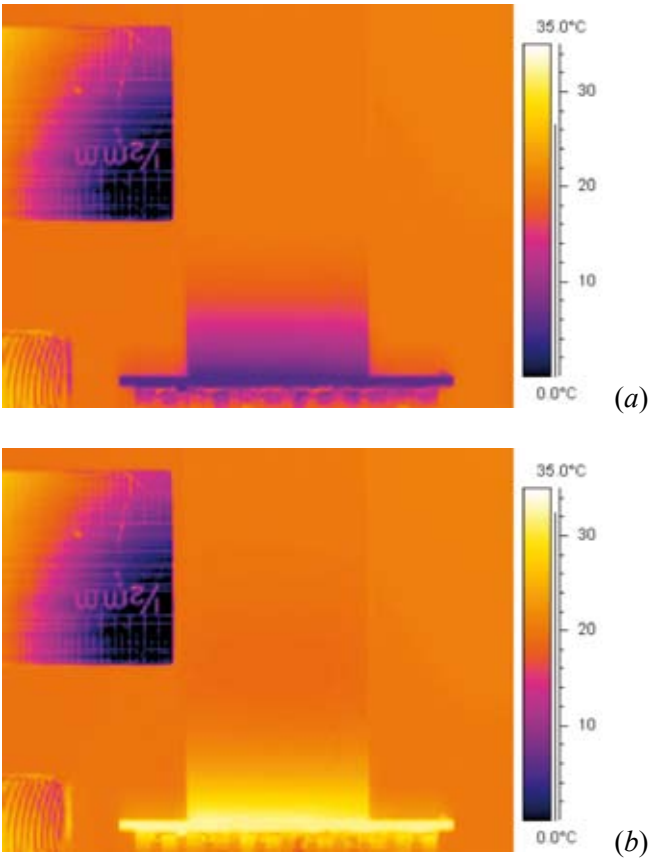


**Figure 12.** (*a*) Temperature profile when the Peltier junction was at its coldest; (*b*) temperature profile when the Peltier junction was at its hottest.

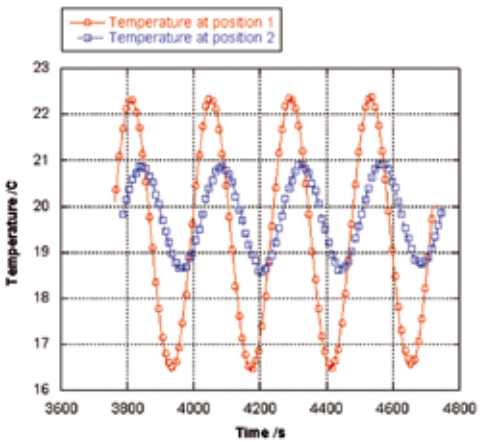


**Figure 13.** Temperature-time profiles at two different positions on the specimen.

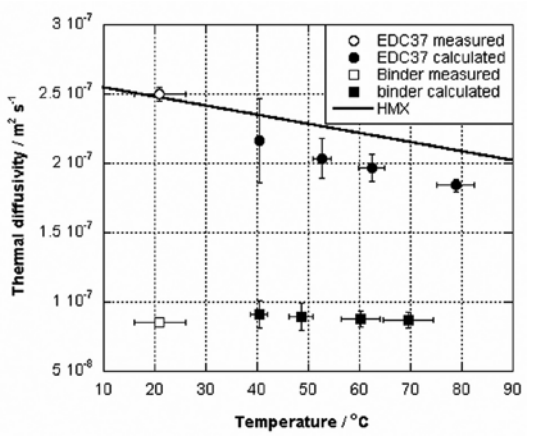


**Figure 14.** Thermal diffusivity results. HMX data taken from Ref. [14].

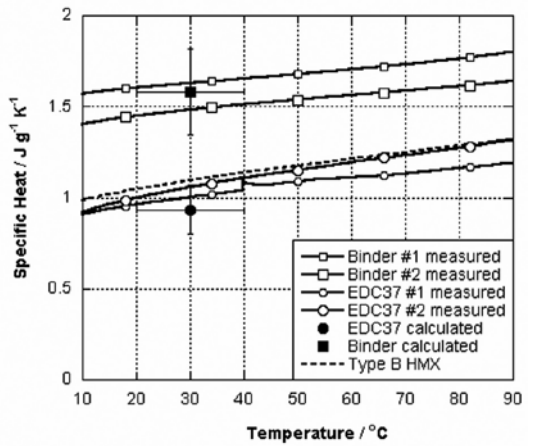


**Figure 15.** Specific heat capacity results.

Note that the plots presented in Figures 11, 14 & 15 contain points that were calculated using equation (2) and data from the other two techniques. It can be seen that there is a good degree of self-consistency, and hence we believe that data obtained by these methods can be relied upon for thermal modelling of processes such as hot-spot growth to deflagration.

**Lead-free (or green) primers and a novel method for assessing them**

Lead styphnate (or more formally 'lead trinitroresorcinate') and lead azide are widely used primary explosives for initiatory systems [23]. Such devices also contain pyrotechnic compounds based on heavy elements such as lead, mercury, barium and antimony. Consequently ejecta and deposited residues inevitably contain toxic compounds, most of which are difficult to remove from the environment where they have been deposited.

Many reports have been produced on the dangerous quantities of lead at firing ranges e.g. [24, 25]. Huynh *et al.* [26] reported that the US Army consumes over 710 lbs (*ca.* 320 kg) of lead from primary explosives each year. Law enforcement operatives and recreational shooters are also exposed to dangerous levels of lead. To address this problem, many new primer mixes are being developed to replace lead-based primary explosives. Thus any search of the patent databases using the key-word phrase 'green primer' yields many thousands of results. Along with this interest in mixes has been the development of new energetic compounds, such as those suggested by Huynh *et al.* [26] and Klapötke *et al.* [27]. For such compounds to be useful replacements for lead styphnate, a comprehensive characterisation study is required.

A large number of methods for testing explosive performance exist [28], so it is important to know which is the most appropriate for a given application. It is well-known that energetic material performance is greatly affected by level of confinement, ambient conditions, and other environmental variables [29]. While constructing rounds and batch firing is the usual method for testing functionality of primers, there are many factors affecting the output of such a system. To remove test condition variability and progress the development of primer compositions, a direct method of primer performance evaluation is required.

To meet this goal, an instrumented primer testing facility has been designed and built to simulate and control the conditions experienced by primers contained within ammunition. Physical data obtained from the facility, when compared with data from live fire tests, can give a greater understanding of which primer characteristics are important to functionality.

The system comprises three discrete sections: (i) a gas-gun to propel an impactor; (ii) a projectile; and (iii) an experimental space suitable for the safe handling of energetic materials (see Figure 16). The arrangement is modular allowing each section to be adapted to many different types of experiment.

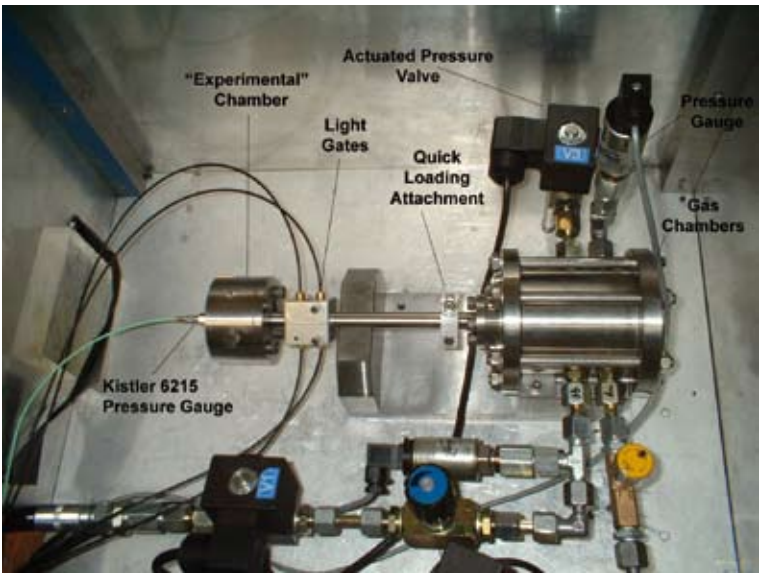


**Figure 16.** Photograph of the experimental set-up.

The propulsion system of the gas-gun consists of a reservoir that can be pressurized to 80 bar with either nitrogen, air or helium. The stainless steel barrel used in the experiments reported here is 150 mm in length, with a bore of 4.4

mm and a wall thickness of 5 mm. The velocity of the projectile is measured using light gates at the muzzle of the barrel.

The current investigation concerns replacement primers for training ammunition (see Figure 17). Training ammunition allows military and law enforcement operatives to train with real weapons in live fire scenarios but with a much reduced risk of injury. One design consists of a two primer system, instead of primer and propellant. A rear percussion primer propels a small nylon ball within the round, which subsequently impacts and ignites a front primer. The front primer propels a lightweight, paint-carrying projectile. Primer characterisation is crucially important here. The apparatus shown in Figure 16 proved capable of firing a 4.6 mm diameter nylon ball of mass 70 mg at velocities of between 200 and 500 m $s^{-1}$. Barrels of different dimensions can be inserted in order to fire projectiles that simulate the impactor of interest.

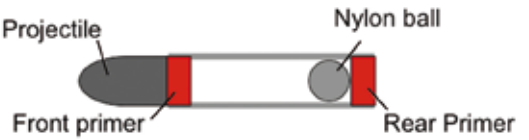


**Figure 17.** Schematic cross-section of a round of one particular training ammunition.

Three types of 5.56 mm centre-fire boxer primers (see Table 1) were tested in the configuration described above. While the primary aim was to investigate heavy-metal-free primers, lead styphnate-based primers were also tested in order to compare the performance of novel compositions against a known system. 'EPPCM' was previously developed for training ammunition through progressive continual shooting of live rounds. The system described here aims to speed up the development of mixes such as this, as no additional assembly is required.

**Table 1.** Primer compositions tested

| | |
|---|---|
| Primer A | A lead styphnate based boxer primer. Contains 18 mg Net Energetic Content (NEC) and cover foil |
| Primer B | Heavy-metal-free mix from the same supplier as 'Primer A'. Also a boxer primer with 8 mg NEC and foil |
| 'EPPCM' | 'Experimental Phosphorus / Potassium Chlorate Mix'. This contains a mixture of red phosphorus and potassium chlorate with stabilisers and binders. All held within a primer cup, no anvil or foil, 22 mg NEC |

When the ball impacts, the primer ignites/detonates and gases are released into a cavity. The dimensions of this cavity imitate those of a primer situated behind a projectile in the training round under investigation. In order to quantitatively assess the primer mixes, the pressure output from primer cups was directly measured using a Kistler 6215 quartz high-pressure gauge aligned face-on to the open face of a primer cup. This gauge is the NATO standard gauge for ballistic measurements up to 6,000 bar. The pressure gauge has a sensitivity of 1.46 pC/bar and was connected to a Kistler 5011 charge amplifier. The output from the amplifier is recorded and subsequently analysed to produce a pressure-time curve (or 'pressure profile') from which many parameters may be computed, such as: maximum pressure, rate of pressure rise and time to maximum pressure since impact. It is instructive to measure these parameters, as they have direct effects on primer and, by extension, ammunition functionality within a live round.

Nine primers from each batch studied were impacted at velocities between about 350 and 450 m $s^{-1}$. No significant effect of the impact velocity was seen on the pressure profiles within this velocity range. Plots of each dataset are presented in Figure 18, with Figure 18(*d*) showing the mean pressure profile of each primer batch.

Oscillations can be seen to be present on all traces. Spectral analysis showed the dominant frequency to be about 265 ± 30 kHz. This includes the documented natural frequency of the gauge. It can be concluded that all oscillations of this type are an artifact due to the resonant response of the transducer. However, simulations performed by Rahman et al. [30] showed that for pressure transducers in this configuration, excitation of mechanical frequencies does not significantly alter the measured peak pressure.

The 'mean pressure profiles' presented in Figure 18(*d*) were calculated on a point by point basis, by taking the mean over all samples for each primer mix at the corresponding time. The motivation for doing this is to give an overall comparative idea of how each primer responds. The error on the mean gives an indication of the spread in the data, and hence the repeatability of primer performance.

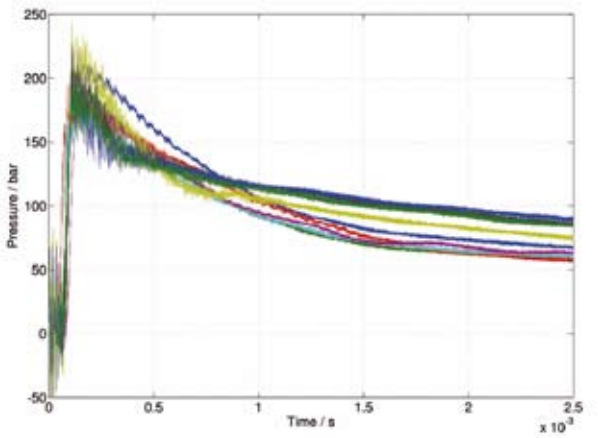


(*a*)

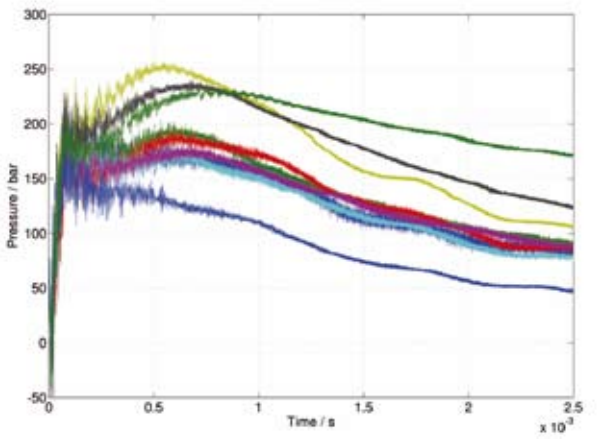


(*b*)

**Figure 18.** (first part)
(*a*) Pressure-time profiles for ‘Primer A’.
(*b*) Pressure-time profiles for ‘Primer B’.

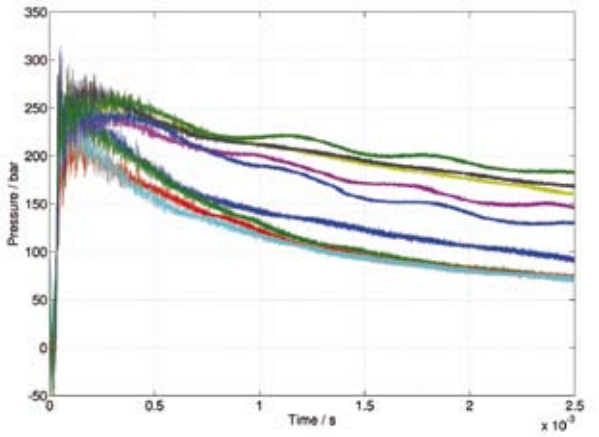


(*c*)

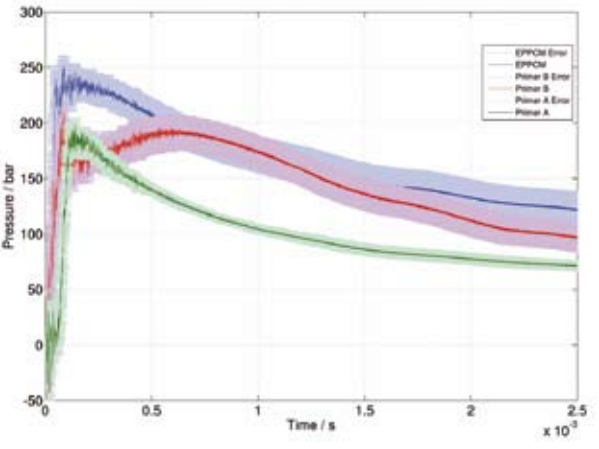


(*d*)

**Figure 18.** (second part)
(*c*) Pressure-time profiles for primer 'EPPCM'.
(*d*) Mean of each dataset and error to indicate spread of results.

The shape of the pressure profile is very similar for all the traces, rising sharply up to a peak, followed by an exponential-like decay to a pressure higher than ambient. This is in agreement with the shapes of the traces presented by Doru *et al.* [31] and Rahman *et al.* [30]. It is believed that the sharp pressure rise is dominated by the formation of hot gases from primer ignition, and the decay time is a characteristic of the cavity.

The maximum pressures from primers A, B, and EPPCM were approximately 175, 180, and 240 bar respectively. The times after impact required to reach this maximum pressure were approximately 150, 90, and 50 μs, respectively, with primer A showing the largest variation. A secondary peak is seen on the pressure-time traces for primer B (see Figure 18*b*). This can be seen to vary considerably shot-to-shot, indicating the presence of different burn rates within the mix, but starts about 600 μs after impact.

The results presented provide good evidence that the system is working appropriately, and give confidence that development of the technique is worth continuing. Some of the parameters we intend to investigate are: energetic content, energetic volume, pressing pressure, anvil design, impactor velocity, primer shape, and ambient conditions. As the motivation for this research is the investigation of heavy-element-free mixtures, energetic content is the primary concern.

There are a number of possibilities for further types of measurement. The design of the system allows for this. Primer ignition temperatures and heat output would be useful parameters to measure. To this end, a pyrometric experimental module is under development in order to investigate burn temperatures, how they can be controlled, and what effect this has on ammunition.

The amount of debris generated from the primer is also of interest because explosive residue may impede reloading. Also the ejecta gives clues as to the quality of the primer ignition. For this reason, a combination of high-speed photography and laser analysis of ejecta is currently underway.

**RDX morphology and its shock sensitivity**

The published literature concerning which factors influence the shock sensitivity of granular explosives presents a somewhat confusing picture. A particular problem is that the results of different studies often cannot be directly compared due to the different methods and criteria used to determine sensitivity. For example the order of sensitivity obtained from wedge tests may be different to that determined from gap-testing [32-34]. These variations are caused primarily by the difference in nature of the incident shock in different tests which cause reaction to occur. The duration and magnitude of the incident shock strongly influence the dominant mode of hot-spot formation, promoting some modes and causing others to be suppressed [35-37]. The subsequent growth and spread of reaction is also heavily influenced by the shock pressure.

In order to identify the most important crystal features that cause hotspots to develop in a granular explosive, we investigated various batches of tapped granular RDX (cyclotrimethylenetrinitramine) having a wide range of crystal

shapes, void contents and surface qualities. Two main factors were considered – the first concerns the compaction properties of the materials, because the sensitivity may be affected by the strength of the material and the amount of energy released during crystal fracture. The second is concerned with the shape and size of the crystals – detailed information about individual crystal morphology was obtained through computer analysis of optical microscope images. The effect of particle size was studied by sieving the crystals into three different size classes within the range 10-1600 μm (see Table 2). The morphology of the batches was examined in detail and their sensitivity to shock was assessed using a small-scale gap test developed in our laboratory by Chakravarty, Czerski and co-workers [38-40]. The effect of loading rate on compressibility was also studied and whether there was a correlation with sensitivity.

RDX is a high performance, crystalline, secondary explosive. In its various applications (mostly military) it is usually mixed with other explosives and a polymer binder and pressed into high-density powder compacts for use either as a polymer-bonded explosive (PBX) or a propellant. RDX is produced in crystalline form by one of two different manufacturing processes. The Woolwich or 'nitric acid' process (referred to in this paper as 'Type I') produces almost pure RDX with few impurities. The Bachmann or 'aceto-nitric' process (referred to in this paper as 'Type II') produces mixed products of approximately 79% RDX, 6% HMX and 15% intermediates. There has been found to be considerable variation between batches from the various manufacturers as measured by gap, critical diameter, wedge, and fragment impact tests. The explanation for these differences appears to lie in the crystal and bed morphology rather than in any differences in chemical composition or crystal structure, but a major problem is that precise information on the manufacturing processes and subsequent treatment of the samples is usually not known. Even within a given factory, different processes may be used to produce batches with different particle sizes. The non-uniformity of this granular material leads to an extremely complex situation with large stress and temperature variations possible on a scale of micrometers.

Czerski investigated a range of possible factors including internal void content, particle size and the physical appearance but was unable to identify a single dominant factor. Other authors have suggested that factors that should be considered include the HMX content [41], the number of inter-granular voids [42], the number and size of internal defects (results here appear somewhat contradictory [43, 44]) and the particle size [45, 46]. Khasainov *et al.* [46] published a review summarising the effect that particle size, or more importantly specific surface area, has on the sensitivity of a range of explosives. They suggested that in the majority of the cases they studied there was a strong

relationship between run distance to detonation/critical diameter and the specific surface area. In most cases those materials which were more sensitive were found to have a greater specific surface area. However, in cases where the shock is of a very short duration it is often found that finer grain material is less sensitive [47, 48].

**Table 2.** Details of the various batches of RDX studied

| Size Class | Manufacturer | Type | % HMX | Melting point/ °C | Tapped density / %TMD |
|---|---|---|---|---|---|
| Class 5 10-30 μm | Dyno | I | 0.9 | 201.9 | 50 ± 1 |
| | Bridgwater | II | 7.3 | 199.0 | 32 ± 1 |
| | Bridgwater | I | 0.0 | 206.0 | 43 ± 1 |
| | SME | II | 0.0 | 205.0 | 38 ± 1 |
| Class 1 100-300 μm | Dyno | I | 1.0 | 200.7 | 62 ± 1 |
| | Bridgwater | I | 8.0 | 194.0 | 62 ± 1 |
| | SME | II | 0.0 | 205.0 | 61 ± 1 |
| Class 4 600-1500 μm | Dyno | I | 0.3 | 202.6 | 65 ± 1 |
| | Bridgwater | I | 0.0 | 205.0 | 65 ± 1 |
| | Bridgwater | II | 4.1 | 198.3 | 64 ± 1 |
| | SME | II | 0.0 | 205.0 | 61 ± 1 |

The reason suggested for this cross-over is that for very short duration shocks the time to ignition is more critical than the time to growth of detonation, and coarser grains are easier to ignite and so have an increased sensitivity. For longer duration shocks where the time to ignition is less important, an increased specific surface area, corresponding to a finer particle size, leads to an increased burning surface area and therefore a more rapid transition from deflagration to detonation (DDT). It is therefore clearly important when measuring the sensitivity of granular explosives to differentiate between the sensitivity to ignition (i.e. at what point burning starts) and the sensitivity to detonation (i.e. at what subsequent point does DDT occur).

Gap testing was used to determine the probability that an incident shock would initiate the RDX. An RP80 detonator was used to provide a reproducible shock and a layer of PMMA was placed between the end of the detonator and the charge (Figure 19). Varying the thickness of the PMMA ‘gap’ directly changes the shock pressure which reaches the charge. By carrying out a series of experiments, it was possible to find the critical gap thickness. This represents the largest gap and smallest shock which can be used while still satisfying an initiation criterion. The results are shown in Figures 20 and 21.

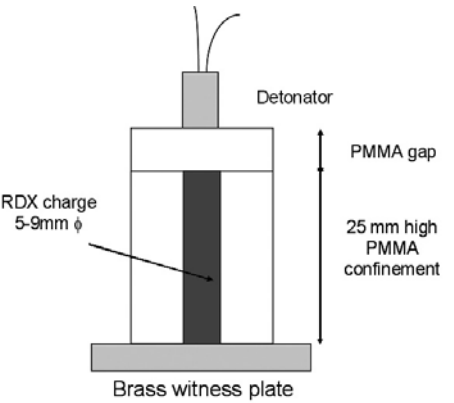


**Figure 19.** Schematic diagram of gap test used.

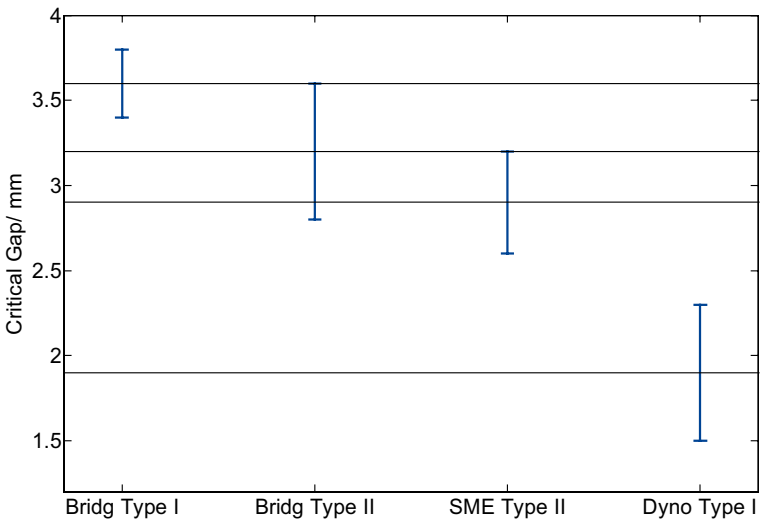


**Figure 20.** The order of sensitivity determined for granular RDX from various manufacturers having a size range of 600-1500 μm (Class 4).

The compressibility of the granular RDX was determined at two loading rates using an Instron and a drop-weight machine. Our drop-weight facility consists of a 6.414 kg aluminium mass which can be dropped from a height of up to 1.2 m. The falling weight is guided by two external steel guide rods to the impact point. Velocities of up to 5 m $s^{-1}$ can be achieved at impact generating strain rates in the range of a few hundred to a few thousand per second, depending on specimen size.

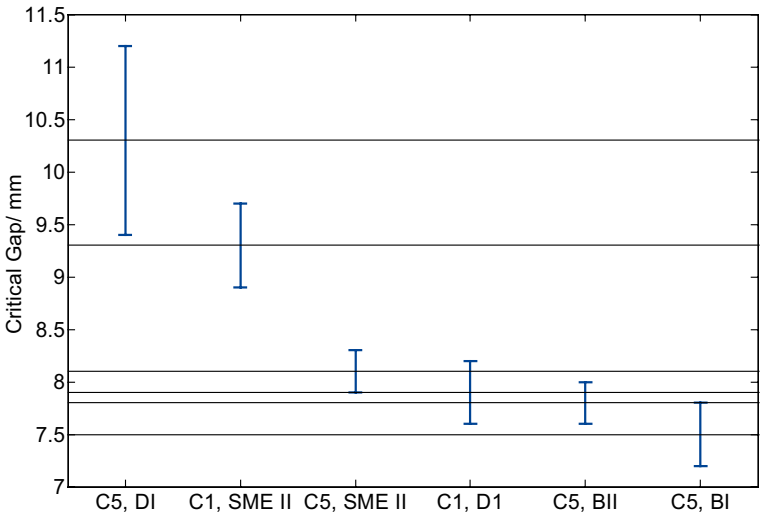


**Figure 21.** The order of sensitivity determined for granular RDX from various manufacturers having two size ranges: C1 (Class 1) 1-30 mm, C5 (Class 5) 100-300 μm.

The sample cell is shown schematically in Figure 22. It consists of a hollow steel cylinder (with an internal diameter of 10 mm), a removable steel end cap and a freely moving steel plunger. The diameter of the plunger was equal to the internal diameter of the cylinder to within a few tens of microns. This is important as it prevents fine material from escaping from the holder during compression.

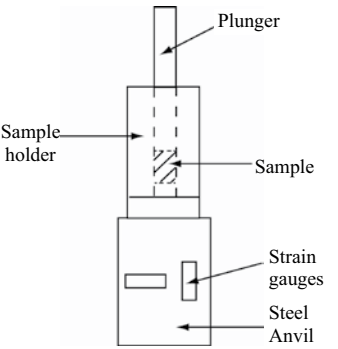


**Figure 22.** Schematic diagram of granular material compression cell.

Drop-weight traces generally contain oscillations caused by vibrations. Such vibrations are unavoidably excited by the impact of the weight. Some

success in reducing their amplitude has been achieved using pulse shaping during experiments on softer samples [49]. In those experiments it was found that most of the noise could be removed by performing a fast Fourier transform and then filtering the Fourier spectrum to remove a small range of high frequency components. Examples of density versus pressure traces calculated both from the raw data and from filtered data are shown in Figure 23.

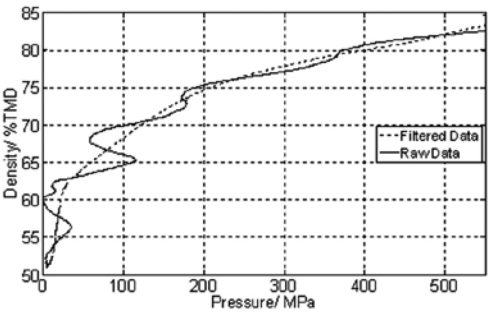


**Figure 23.** Density versus pressure curves for a Class 5 material showing the large improvement in signal quality and reduction in oscillations when using Fourier filtered data.

For each batch of RDX three dynamic and three quasistatic compression experiments were performed. In each experiment material was gradually added to the cell with regular and vigorous tapping of the container on a hard surface. Sufficient material was added in each case to give a final column height of 15 mm. The crosshead speed of the Instron was set to 4 mm/min. The maximum load applied was 10 kN. The machine compliance of the Instron was determined by applying a load to the compression cell empty. The compliance so determined was used to correct the quasistatic RDX data.

For a given batch of RDX there were found to be variations of up to 10% in the mechanical properties as determined from these compaction experiments. This level of variation is to be expected for granular materials such as these where the bed morphology will differ in each experiment. Quasistatic density versus pressure curves obtained using the Instron for some of the Class 4 and Class 5 materials are presented in Figure 24.

Comparing Figures 24*a* and *b* it can be seen that there are clear differences in the quasistatic response of the Class 4 and Class 5 materials. The Class 4 materials, which had considerably higher initial tapped densities than the Class 5 materials, are compacted to within 95-100% of the theoretical maximum density (TMD) at an applied pressure of 80 MPa. The Class 5 materials, however, only

reached a density of 85-90% of the TMD at this pressure. The Class 5 materials also exhibited a large initial increase in density at low pressure, which is not observed for the Class 4 materials. Given their relatively low initial tapped densities it seems likely this is due to a simple reduction in porosity. Crystal fracture is unlikely to be occurring.

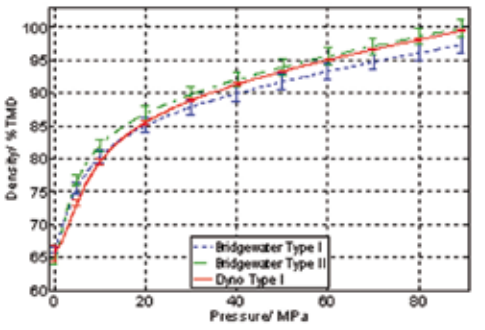


(*a*)

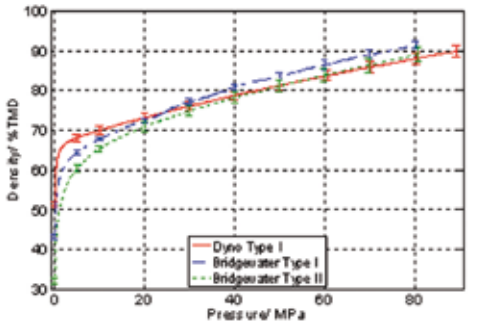


(*b*)

**Figure 24.** (*a*) Quasistatic density-pressure plots for some Class 4 materials. (*b*) Quasistatic density-pressure plots for some Class 5 materials.

It can be seen from Figure 24 that within a given class size there are variations in the properties of the different batches but these are not very significant and do not seem to correlate with the sensitivity at all (compare with Figures 20 and 21). Given this lack of significant variation it seems unlikely that the mechanical strength has a significant influence on the sensitivity within a class size.

The density versus pressure curves obtained from drop-weight and Instron experiments on some Class 4 materials are compared in Figure 25. It is clear that there is a significant difference in the response of the materials at the two compaction rates. In the quasistatic Instron experiments, where the material was

compacted at a rate of 4 mm/s, the samples were compressed to a density of 95-100% of the TMD at a pressure of 90 MPa. When the samples were compacted at an initial rate of 5 m/s in the drop-weight, the density achieved at this pressure was only around 80% of the TMD. Only at pressures of over 700 MPa did the samples approach a density of 95% of the TMD. This large difference in response between the two strain rates was also seen for the other particle size ranges.

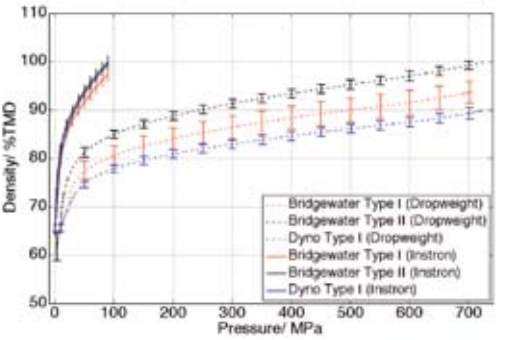


**Figure 25.** A comparison of the quasistatic and dynamic density-pressure responses of various Class 4 RDX powders.

A Malvern Mastersizer 2000 particle size analyser was used to measure the particle size distributions for some of the batches of RDX before and after compaction. It should be noted that in performing this measurement it was assumed that the particles were perfectly spherical. Figure 26 presents the particle size distributions for the Class 4, Bridgwater Type I batch in the as-received condition and after both quasistatic and dynamic compaction. The peak particle size can be seen to be reduced from 1200 μm to between 400 and 500 μm. The distributions for the material recovered after Instron and drop-weight experiments are very similar: both have a peak size of between 400 and 500 μm and a similar shape. This suggests that the differences observed in the compressibility (see Figure 24) in the two different compaction-rate regimes are not due to differences in crystal fracturing. Rather it is likely that the observed differences in compressibility are due to the length of time that the fractured particles have to move into an equilibrium arrangement. At quasistatic rates, the material has a relatively large amount of time to move around and pack together more densely. In the dynamic experiments, where the compaction happens several orders of magnitude more quickly, the material does not have sufficient time to achieve an equilibrium arrangement. Instead the material appears to ‘lock up’ and hence reaches considerably lower densities.

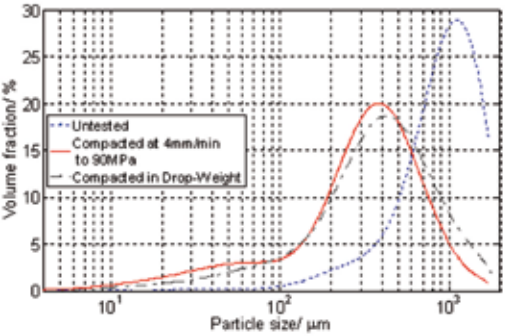


**Figure 26.** Particle size analysis of Class 4, Bridgwater Type I RDX as received and after quasistatic and dynamic compaction.

An optical microscope was used to take digital photographs of batches of Class 1 (100-300 µm) and Class 4 (600-1500 µm) RDX. A computer program called ImageJ was used to analyse the photographs and investigate individual crystal morphology. The program provides information on a range of variables including the surface area, perimeter, Feret number, which is the length of the longest straight line that can be drawn between any two points on the perimeter of the particle, circularity, which is defined as:

$$circularity = 4\pi \frac{Area}{(Perimeter)^2} \tag{5}$$

(a circularity value of unity corresponds to a perfect circle), and the ellipticity, which is the ratio of the Feret number to the length of the major axis (an ellipse has an ellipticity of unity).

The program can also fit ellipses to the projected images of the particles. Examples of various stages in the image processing are shown in Figure 27. Note that any particles that intersect the edge of the frame are ignored. Between 800 and 1000 particles were analysed for any given batch of RDX, corresponding to between 20 and 35 photographs per batch. For the Class 4 materials this corresponds to between 10% and 15% of the total volume of material used in the gap tests reported by Czerski & Proud [50]. Data on a range of parameters obtained from analysis of optical microscope images is presented in Table 3.

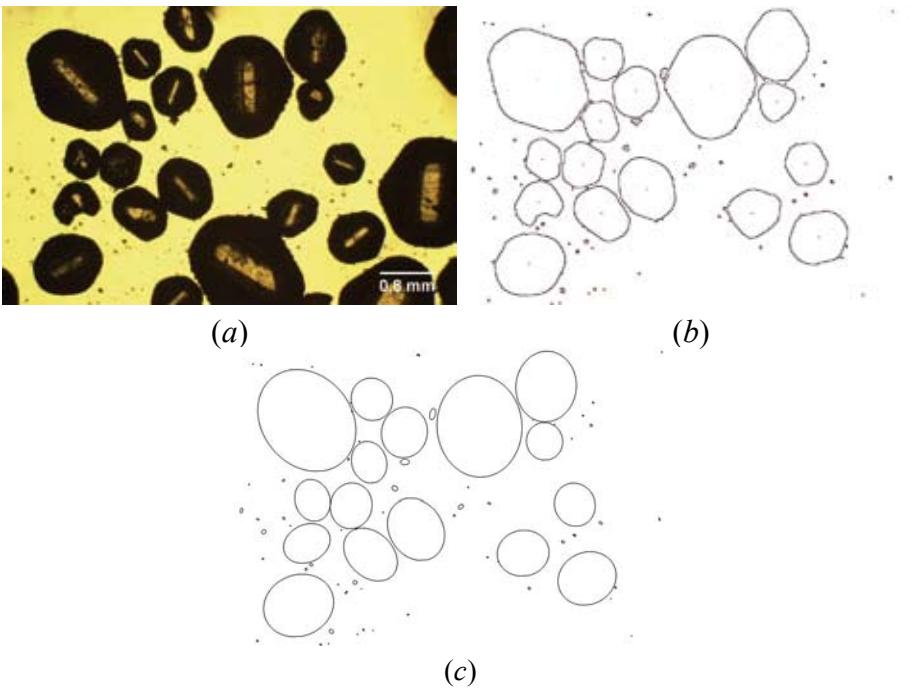


**Figure 27.** (*a*) Optical micrograph of some Class 4, Dyno Type I RDX.
(*b*) Outlines of the particles shown in (*a*) determined using ImageJ.
(*c*) Particle ellipses for the particles shown in (*a*) calculated using ImageJ.

The columns in Table 3 are arranged, within a class size, by sensitivity such that moving to the right represents a reduction in sensitivity as measured by small-scale gap-testing. The rows highlighted in red show parameters that appear to scale with the sensitivity. The two measurements of size, the Feret number and the length of the minor axis, can be expressed as a simple numerical average over the total number of particles and also as the average size determined from the area fraction (*i.e.* the sum of the area fraction multiplied by particle size). As can be seen in Figure 28 these two methods of calculation can give considerably different results. All the parameters that appear to scale with the sensitivity are connected with the ratio between the area of a particle and its physical size. It seems that the sensitivity is reduced for batches where a greater fraction of the total area is contributed by larger particles. In three dimensions, the appropriate ratio would be that between the surface area of the particle and its volume, *i.e.* the specific surface area.

**Table 3.** Particle data obtained using ImageJ

| | Class 4 | | | Class 1 | |
|---|---|---|---|---|---|
| | Bridgwater I | Bridgwater II | Dyno I | SME II | Dyno I |
| Average particle area/ $mm^2$ | 0.254 | 0.225 | 0.325 | 0.0123 | 0.0106 |
| Circularity | 0.677 | 0.593 | 0.726 | 0.674 | 0.607 |
| Feret number (by number)/ mm | 0.478 | 0.409 | 0.561 | 0.133 | 0.0798 |
| Feret number (by area)/ mm | 1.081 | 1.226 | 1.434 | 0.196 | 0.336 |
| Minor axis (by number)/ mm | 0.352 | 0.298 | 0.410 | 0.0936 | 0.0553 |
| Minor axis (by area)/ mm | 0.872 | 1.003 | 1.177 | 0.170 | 0.258 |
| Peak of area fraction vs. minor axis/ mm | 0.98 | 1.05 | 1.33 (m), 0.75 (s) | 0.16 | 0.30 |
| Ellipticity | 1.07 | 1.10 | 1.07 | 1.05 | 1.11 |

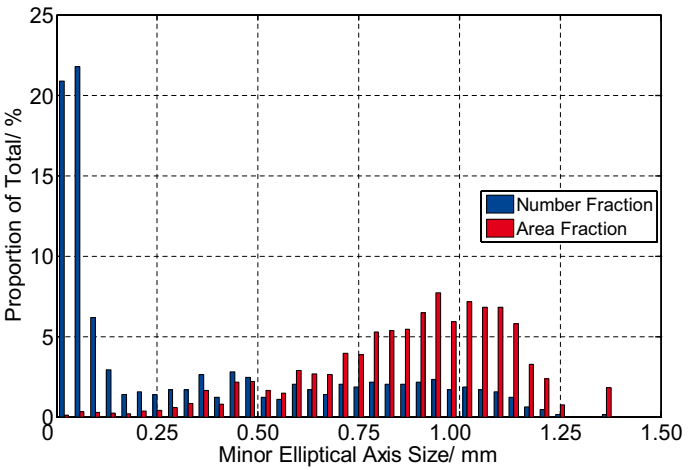


**Figure 28.** Histogram showing particle size data for Class 4, Bridgwater Type I RDX.

An estimate of the specific surface area can be made by approximating each particle as an ellipsoid formed by rotating its projected ellipse (see Figure 27*c*) around its major axis. Using the data from ImageJ for ellipses fitted to the particles the total surface area and total volume for a given batch can be calculated. The volume can be scaled to determine the equivalent volume the material would occupy at the appropriate tapped density. The initial calculated volume corresponds to material with the crystal density, i.e. 100% TMD. The ratio of the total surface area to this scaled volume gives an estimate of the specific surface area present during the gap tests, subject to the stated assumptions namely that the particles are ellipsoids and have perfectly smooth surfaces. Data for some of the RDX materials studied is presented in Table 4.

In order to verify that a sufficient number of particles had been analysed in each case to make the sample representative of the batch as a whole the same analysis was run on half of the total number of particles. The difference between the two calculated specific areas then gives an idea of the error involved (this ignores errors associated with the assumptions made during the analysis and outlined above). Calculated values for the specific surface area and the associated error for a range of Class 4 and Class 1 materials are given in Table 4 below. The rows are arranged by sensitivity within a class so that as the table is descended, the sensitivity reduces.

**Table 4.** Specific surface areas of some of the materials

| Class | Manufacturer | Type | Specific surface area/ $m^{-1}$ |
|---|---|---|---|
| 4 | Bridgwater | I | 3880 ± 50 |
| 4 | Bridgwater | II | 3370 ± 120 |
| 4 | Dyno | I | 2850 ± 20 |
| 1 | SME | II | 21700 ± 900 |
| 1 | Dyno | I | 12330 ± 110 |

The data presented in Table 4 is suggestive that within any given class size, the sensitivity of a batch increases as the specific area is increased. Due to the lack of available samples and associated sensitivity data, it is currently not possible to demonstrate this more rigorously. A number of important processes including heat transfer and burning depend heavily on the available surface area. Khasainov *et al*. [46] suggested that if the ratio of the pressure behind the shock wave to the ignition pressure is high, then the formation of hot-spots is fast and the critical hot-spot size is small compared with the median size of heterogeneities. This means that most heterogeneities present in the explosive can form growing reaction centres and hence the area of burning surface is close

to the available specific surface area. In this case the sensitivity of the material will scale with the specific surface area as is observed in this work for the Class 4 and Class 1 materials.

Specific surface area may play a particularly important role in determining the order of sensitivity in the gap tests reported by Czerski & Proud [50] as the order was determined by the DDT boundary rather than the 'no reaction to deflagration' boundary. As the rate at which energy is released by burning, which is vital to determining the likelihood of a DDT occurring, depends on the burning surface area it is perhaps not surprising that the specific surface area plays an important role.

As a note of caution it can be seen from Figure 20 that the differences in sensitivity between the Class 1 and Class 5 materials do not seem as simple to explain. The Class 5 materials will have a larger specific surface area than the Class 1 materials but are not necessarily more sensitive (because of the small crystal size and difficulty in separating out the crystals it was not possible to investigate the crystal morphology of the Class 5 materials in the way described earlier). A possible explanation for this inconsistency is that, for the given conditions of the gap tests, the Class 5 materials are small enough that the relative pressure is lower. In this case the time to ignition would become more relevant and the burning surface would no longer scale with the specific surface area.

In conclusion it has been shown that the sensitivity of Class 4 and Class 1 RDX to a DDT in small-scale gap testing appears to scale, within a given class size, with the specific surface area. It has also been shown that the mechanical properties of RDX are strongly rate dependent. There was a markedly different response of the material to compaction at a high rate compared to a low rate. Particle size analysis showed that the extent of crystal fracture occurring in the two cases was comparable suggesting the difference in response was down to the length of time fractured crystals had to arrange themselves into an equilibrium arrangement.

In order to investigate the possible effect of voids within crystals on sensitivity, samples of crystals from various batches that had been placed within an index-matched fluid were examined with an optical microscope. Any closed internal voids show up as black due to the impedance mismatch. The average number of voids (as projected onto a 2D plane) contained in crystals of each material was thus determined. Selected results are shown in Tables 5 and 6. It can be seen that there was no clear correlation between the void content and the order of sensitivity determined from small-scale gap testing.

**Table 5.** Comparison of critical gap with average number of voids for Class 5 materials

| Sample | Dyno Type I | SME Type II | Bridgwater Type II | Bridgwater Type I |
|---|---|---|---|---|
| Critical gap/ mm | 10.3 | 8.1 | 7.8 | 7.5 |
| Average number of voids | 4.1 | 1.5 | 3.1 | 0.1 |
| Mode void number | 0 | 0 | 2 | 3 |

**Table 6.** Comparison of critical gap with average number of voids for Class 1 materials

| Sample | SME Type II | Bridgwater Type II | Bridgwater Type I |
|---|---|---|---|
| Critical gap/ mm | 9.3 | 8.5 | 7.9 |
| Average number of voids | 165 | 177 | 237 |

In conclusion, the various methods available for measuring sensitivity cover a wide range of shock magnitudes and durations. It is therefore unlikely that one single factor will determine the order of sensitivity across all methods or for all particle sizes and morphologies. For the gap tests reported here, the void content appears not to be a determining factor. Other factors such as the specific surface area and particle size seem more important in determining the order of sensitivity. A number of processes such as heat transfer and burning depend strongly on the surface area so it is perhaps not surprising that this parameter has been shown to have a considerable effect on the sensitivity.

**Acknowledgements**

The British Ministry of Defense are thanked for their support of our research on energetic materials over many years. The Engineering and Physical Sciences Research Council (EPSRC) are thanked for the loan of an infrared camera. JWA also thanks the EPSRC for a studentship. We would like to thank past and present members of the Cavendish Laboratory's mechanical and electronic workshops for assistance with the design and construction of apparatus and specimens required for these experiments.

## References


[1] Church P.D., Townsley R., Bezance T., Proud W.G., Grantham S.G., Bourne, N.K., Millett J.C.F., Simulation of Precise Setforward and Setback Experiments, *Int. J. Impact Engng*, **2005**, *32*, 80-91.

[2] Huntington-Thresher W., Church P.D., Kosecki A., Gower B., Gould P., Proud W.G., Chapman D., Response of PBXs and Inert Substitutes in Launch and Impact Scenarios, *J. Phys. IV France*, **2006**, *134*, 231-236.

[3] Williamson D.M., Siviour C.R., Proud W.G., Palmer S.J.P., Govier R., Ellis K., Blackwell P., Leppard, C., Temperature-Time Response of a Polymer Bonded Explosive in Compression (EDC37), *J. Phys. D: Appl. Phys.*, **2008**, *41*, 085404.

[4] Siviour C.R., Laity P.R., Proud W.G., Field J.E., Porter D., Church P.D., Huntingdon-Thresher W., High Strain Rate Properties of a Polymer-Bonded Sugar: Their Dependence on Applied and Internal Constraints, *Proc. R. Soc.*, **2008**, *A464*, 1229-1255.

[5] Williamson D.M., Palmer S.J.P., Proud W.G., Govier R., Brazilian Disc Testing of a UK PBX Above and Below the Glass Transition Temperature, in: *Shock Compression of Condensed Matter - 2007*, (M. Elert, M.D. Furnish, R. Chau, N. Holmes, J. Nguyen, Eds.), American Institute of Physics, Melville NY **2007**, pp. 803-806.

[6] Williams M.L., Landel R.F., Ferry J.D., The Temperature Dependence of Relaxation Mechanisms in Amorphous Polymers and Other Glass-Forming Liquids", *J. Amer. Chem. Soc.*, **1955**, *77*, 3701-3707.

[7] Thompson D.G., Olinger B., DeLuca R., The Effect of Pressing Parameters on the Mechanical Properties of Plastic Bonded Explosives, *Propellants*, *Explos. Pyrotech.*, **2005**, *30*, 391-396.

[8] Huntley J.M., Laser Speckle and Its Application to Strength Measurement and Crack Propagation, *PhD thesis*, Univ. of Cambridge **1986**.

[9] Goldrein H.T., Huntley J.M., Palmer S.J.P., Whitworth M.B., Field J.E., Optical Techniques for Strength Studies of Polymer Bonded Explosives, in: *Proc. 10th Int. Detonation Symposium*, (J.M. Short, D.G. Tasker, Eds.), Office of Naval Research, Virginia, Arlington **1995**, pp. 525-535.

[10] Goldrein H.T., Applications of Optical Strain-Measurement Techniques to Composite Materials, PhD thesis, Univ. of Cambridge **1996.**

[11] Sjödahl M., Benckert L.R., Electronic Speckle Photography: Analysis of an Algorithm Giving the Displacement with Subpixel Accuracy, *Appl. Opt.*, **1993**, *32*, 2278-2284.

[12] Awaji H., Sato S., Diametral Compressive Testing Method, *Trans. ASME: J. Engng Mater. Technol.*, **1979**, *101*, 139-147.

[13] Carneiro F.L., Barcellos A., Résistance à la Traction des Bétons, *RILEM Bull.*, **1949**, *13*, 98-125.

[14] Hanson-Parr D.M., Parr T.P., Thermal Properties Measurements of Solid Rocket Propellant Oxidizers and Binder Materials as a Function of Temperature, *J. Energ.*

*Mater.*, **1999**, *17*, 1-48.
[15] Palmer S.J.P., Williamson D.M., Proud W.G., Bauer, C., Thermal Properties of a UK PBX and Binder System, in: *Shock Compression of Condensed Matter - 2007*, (M. Elert, M.D. Furnish, R. Chau, N. Holmes, J. Nguyen, Eds.), American Institute of Physics, Melville NY **2007**, pp. 849-852.
[16] Carslaw H.S., Jaeger J.C., *Conduction of Heat in Solids*, Oxford University Press, Oxford **1947**, p. 8.
[17] Lees C.H., On the Thermal Conductivities of Crystals and Other Bad Conductors, *Phil. Trans. R. Soc. Lond.*, **1892**, *A183*, 481-509.
[18] Price D.M., Jarratt, M., Thermal Conductivity of PTFE and PTFE Composites, *Thermochim. Acta*, **2002**, *392*, 231-236.
[19] Gandia V., Lopez-Baeza E., A Low-Cost Thermal Diffusivity Measuring Apparatus, *J. Phys. E: Sci. Instrum.*, **1988**, *21*, 757-759.
[20] Musicio A., Bison P.G., Marinetti, S., Grinzato E., Thermal Diffusivity Measurement in Slabs Using Harmonic and One-Dimensional Propagation of Thermal Waves, *Int. J. Thermal Sci*., **2004**, *43*, 453-463.
[21] Sidles P.H., Danielson G.C., Thermal Diffusivity of Metals at High Temperatures, *J. Appl. Phys.*, **1954**, *25*, 58-67.
[22] Parrott J.E., Stuckes A.D., Thermal Conductivity of Solids, London, Pion **1975**, p. 26.
[23] Meyer R., *Explosives* (Third Edition), VCH Verlag, Germany, Weinheim **1987**, pp. 212-213.
[24] Fischbein A., Rice C., Kon S.H., Petrocci M., Selikoff, I.J., Exposure to Lead in Firing Ranges, *J. Amer. Medical Assoc.*, **1979**, *241*, 1141-1144.
[25] Valway S.E., Martyny J.W., Miller J.R., Cook M., Mangoine, E.J., Lead Absorption in Indoor Firing Ranges, *Amer. J. Public Health*, **1989**, *79*, 1029-1032.
[26] Huynh M.H.V., Hiskey M.A., Meyer T.J., Wetzler M., Green Primaries: Environmentally Friendly Energetic Complexes, *Proc. Nat. Acad. Sci. USA*, **2006**, *103*, 5409-5412.
[27] Klapötke T.M., Sabaté C.M., Welch J.M., Alkali metal 5-nitrotetrazolate salts: Prospective replacements for service lead(II) azide in explosive initiators, *Dalton Trans.*, **2008**, 6372-6380.
[28] *Encyclopedia of Explosives and Related Items*, (Fedoroff B.T., Ed.), Picatinny Arsenal, Dover NJ **1960**, Vol. 1, pp. VII-XXVI.
[29] Bailey A., Murray S.G., *Explosives, Propellants and Pyrotechnics*, Chapter 4, Brassey's (UK) Ltd., Oxford **1989**, 59-77.
[30] Rahman S., Timofeev E., Kleine H., Pressure Measurements in Laboratory-Scale Blast Wave Flow Fields, *Rev. Sci. Instrum.*, **2007**, *78*, 125106.
[31] Doru G., Traian R., Viorel T., Teodora Z., Ballistic Performances of Primers: A New Experimental Method for Evaluation, in: *Proc. 10th Seminar on New Trends in Research of Energetic Materials*, (J. Ottis and M. Krupka, Eds.), Czech Republic, University of Pardubice, Pardubice **2007**, pp. 607-615.
[32] Watt D., Peugeot F., Doherty R., Sharp M., Topler D., Tucker, D., Reduced

Sensitivity RDX: Where Are We? in: *Proc. 35th Int. Ann. Conf. of Institut für Chemische Technologie*", Fraunhofer Institut für Chemische Technologie, Germany, Karlsruhe **2004**, paper 9.

[33] Doherty R.M., Nock L.A., Watt D.S., Reduced Sensitivity RDX Round Robin Program: Update, in: P*roc. 37th Int. Ann. Conf. of Institut für Chemische Technologie*, Fraunhofer Institut für Chemische Technologie Germany, Karlsruhe **2006**, paper 5.

[34] Doherty R.M., Watt D.S., Relationship Between RDX Properties and Sensitivity, *Propellants, Explos. Pyrotech.*, **2008**, *33*, 4-13.

[35] Bowden F.P., Gurton O.A., Birth and Growth of Explosion in Liquids and Solids Initiated by Impact and Friction, *Proc. R. Soc. Lond.*, **1949**, A198, 350-372.

[36] Bourne N.K., Field J.E., Bubble Collapse and the Initiation of Explosion, *Proc. R. Soc. Lond.*, **1991**, *A435*, 423-435.

[37] Field J.E., Walley S.M., Proud W.G., Balzer J.E., Gifford M.J., Grantham S.G., Greenaway M.W., Siviour C.R., The Shock Initiation and High Strain Rate Mechanical Characterization of Ultrafine Energetic Powders and Compositions, *Mater. Res. Soc. Symp. Proc.*, **2004**, *800*, 179-190.

[38] Chakravarty A., Proud W.G., Field J.E., Small Scale Gap Testing of Novel Compositions, in: *Shock Compression of Condensed Matter - 2003*, (M.D. Furnish, Y.M. Gupta, J.W. Forbes, Eds.), American Institute of Physics, Melville NY **2004**, pp. 935-938.

[39] Czerski H., Proud W.G., Field J.E., The Relationship Between Shock Sensitivity and Morphology in Granular RDX, *Centr. Europ. J. Energ. Mater.*, **2006**, *3*(3), 3-13.

[40] Czerski H., Proud, W.G., Field, J.E., The Relationship Between Particle Morphology and Sensitivity for Pure Granular RDX, in: *Proc. Thirteenth International Detonation Symposium*, (S. Peiris, R. Doherty, Eds.), Office of Naval Research, Arlington VA **2007**, pp. 581-590.

[41] Oxley J., Smith J., Buco R., Huang J., A Study of Reduced-Sensitivity RDX, *J. Energ. Mater.*, **2007**, *25*, 141-160.

[42] Lecume S., Boutry C., Spyckerelle C., Structure of Nitramines Crystal Defects Relation with Shock Sensitivity, in: *Proc. 35th Ann. Conf. Institut für Chemische Technologie*, Karlsruhe **2004**, paper 2.

[43] Baillou F., Dartyge J.M., Spyckerelle C., Mala J., Influence of Crystal Defects on Sensitivity of Explosives, in: *Proc. 10th Int. Detonation Symposium*, (J.M. Short, D.G. Tasker, Eds.), Office of Naval Research, Virginia, Arlington **1995**, pp. 816-823.

[44] Borne L., Patedoye J.C., Spyckerelle S., Quantitative Characterization of Internal Defects in RDX Crystals, *Propellants, Explos., Pyrotech.*, **1999**, *24*, 255-259.

[45] Moulard H., Kury J.W., Delclos A., The Effect of RDX Particle Size on the Shock Sensitivity of Cast PBX Formulations, in: *Proc. Eighth Symposium (Int.) on Detonation*, (J.M. Short, Ed.), Naval Surface Weapons Center, Maryland, White Oak, Silver Spring **1985**, pp. 902-913.

[46] Khasainov B.A., Ermolaev B.S., Presles H.N., Vidal P., On the Effect of Grain Size on Shock Sensitivity of Heterogeneous High Explosives, *Shock Waves*, **1997**, *7*, 89-105.

[47] Greenaway M.W., Gifford M.J., Proud W.G., Field J.E., Goveas S.G., An Investigation into the Initiation of Hexanitrostilbene by Laser-Driven Flyer Plates, in: *Shock Compression of Condensed Matter - 2001*, (M.D. Furnish, N.N. Thadhani, Y. Horie, Eds.), American Institute of Physics, Melville NY **2002**, pp. 1035-1038.

[48] Walley S.M., Field, J.E., Greenaway M.W., Review: Crystal Sensitivies of Energetic Materials, *Mater. Sci. Technol*., **2006**, *22*, 402-413.

[49] Addiss J., Cai J., Walley S., Proud W., Nesterenko V., High Strain and Strain-Rate Behaviour of PTFE/Aluminium/Tungsten Mixtures, in: *Shock Compression of Condensed Matter - 2007*, (M. Elert, M.D. Furnish, R. Chau, N. Holmes, J. Nguyen, Eds.), American Institute of Physics, Melville NY **2007**, pp. 773-776.

[50] Czerski H., Proud W.G., Relationship Between the Morphology of Granular Cyclotrimethylene-Trinitramine and Its Shock Sensitivity, *J. Appl. Phys.*, **2007**, *102*, 113515.